AD-A075 747 NAVAL RESEARCH LAB WASHINGTON DC F/G 9/1
INTENSE ION BEAM GENERATION WITH AN INVERSE REFLEX TETRODE (IRT--ETC(U)
OCT 79 J A PASOUR , R A MAHAFFEY , J GOLDEN
UNCLASSIFIED NRL-MR-4103 NL

| OF |
AD-
A075747

END
DATE
FILMED
11-79
DDC

LEVEL II

NRL Memorandum Report 4088

Intense Ion Beam Generation with an Inverse Reflex Tetrode (IRT)

J. A. Pasour and R. A. Mosarpur

Science Research Associates
Bladensburg, Maryland 20710

J. Golden and C. A. Kapetanakos

Experimental Plasma Physics Branch
Plasma Physics Division

October 18, 1979

NAVAL RESEARCH LABORATORY
Washington, D.C.

79 10 22

(14) NRL-MR-4103

SECURITY CLASSIFICATION OF THIS PAGE (When Data Entered)

REPORT DOCUMENTATION PAGE

READ INSTRUCTIONS BEFORE COMPLETING FORM

1. REPORT NUMBER: NRL Memorandum Report 4103
2. GOVT ACCESSION NO.
3. RECIPIENT'S CATALOG NUMBER

4. TITLE (and Subtitle): (6) INTENSE ION BEAM GENERATION WITH AN INVERSE REFLEX TETRODE (IRT),
5. TYPE OF REPORT & PERIOD COVERED: Interim report on a continuing NRL problem.
6. PERFORMING ORG. REPORT NUMBER

7. AUTHOR(s): (10) J. A. Pasour*, R. A. Mahaffey*, J. Golden and C. A. Kapetanakos
8. CONTRACT OR GRANT NUMBER(s): (11) 18 Oct 79

9. PERFORMING ORGANIZATION NAME AND ADDRESS: Naval Research Laboratory, Washington, DC 20375
10. PROGRAM ELEMENT, PROJECT, TASK AREA & WORK UNIT NUMBERS: NRL Problem 67H02-28A

11. CONTROLLING OFFICE NAME AND ADDRESS: Office of Naval Research, Arlington, Virginia
12. REPORT DATE: October 18, 1979. (12) 241
13. NUMBER OF PAGES: 13

14. MONITORING AGENCY NAME & ADDRESS(if different from Controlling Office): (9) Memorandum rept.,
15. SECURITY CLASS. (of this report): UNCLASSIFIED
15a. DECLASSIFICATION/DOWNGRADING SCHEDULE

16. DISTRIBUTION STATEMENT (of this Report)

Approved for public release; distribution unlimited.

17. DISTRIBUTION STATEMENT (of the abstract entered in Block 20, if different from Report)

DDC RECEIVED OCT 30 1979 B

18. SUPPLEMENTARY NOTES

*Sachs-Freeman Associates, Bladensburg, Maryland 20710

19. KEY WORDS (Continue on reverse side if necessary and identify by block number)

Ion beams
Inverse reflex tetrode (IRT)
Reflexing electron ion source
Virtual cathode formation

20. ABSTRACT (Continue on reverse side if necessary and identify by block number)

A new reflexing electron ion source is described. The device produces a unidirectional ion beam with relatively high efficiency even when the applied magnetic field exceeds the self field. This new source operates at a low, constant impedance during much of the applied voltage pulse and is better matched to available high-power, low impedance generators than previous reflexing electron devices.

DD FORM 1 JAN 73 1473 EDITION OF 1 NOV 65 IS OBSOLETE
S/N 0102-014-6601

SECURITY CLASSIFICATION OF THIS PAGE (When Data Entered)

251 950 JAB

INTENSE ION BEAM GENERATION WITH AN INVERSE REFLEX TETRODE (IRT)

In recent years, the generation of pulsed, high-current ion beams has attracted much interest because of the large number of applications envisioned for them. These applications include the formation of field-reversing ion rings,[1] inertial confinement fusion,[2] laser excitation,[3] and plasma heating.[4] One class of ion source that has received considerable attention both experimentally[5-10] and theoretically[7,11-13] is that of reflexing electron devices, i.e., reflex triodes[5-8] and reflex tetrodes.[9,10]

In this letter we report on a new reflexing electron ion source and analyze its operation over a wide range of external magnetic field. The most interesting features of the new device are: (i) relatively high efficiency even when the applied magnetic field exceeds the self field, (ii) unidirectionality, and (iii) constant impedance during an appreciable portion of the applied voltage pulse. In addition, the present device can be used in a low-inductance, coaxial geometry to produce solid as well as annular beams. The ions are extracted through the real cathode as opposed to the virtual cathode extraction used in most earlier sources. Consequently, the present device is called an inverse reflex tetrode (IRT). One of the advantages of real cathode extraction is that the zero-potential surface is stationary, flat, and well-defined. On the other hand, the shape and position of the virtual cathode vary with time. Consequently, one would expect that it would be possible to extract "colder" ion beams through a real cathode.

Note: Manuscript submitted September 4, 1979.

Furthermore, we have found that in some instances a proton beam extracted through a virtual cathode is not current neutralized, but with the IRT the beam is almost completely (> 95%) current neutralized.

The IRT has been tested extensively on the Seven Ohm Line (SOL) generator (~ 400 kV, 60 kA) and has been successfully used on the upgraded Gamble II generator as part of the NRL Ion Ring Program. On Gamble II, the IRT has produced 7-8 x 10^{16} protons/pulse with a current efficiency of ~ 50%. These proton pulses have made possible the formation of transient field-reversed ion rings.

A schematic diagram of the IRT (as used on SOL) coupled to an external circuit representing the generator is shown in Fig. 1. The 5 cm diam anode foil A (typically polyethylene) is attached to one end of a stainless steel anode stalk. The other end of the stalk contains a back plate G and is connected to the generator. An external axial magnetic field B_0 is supplied by pulsed solenoidal magnets. Electrons are emitted from the 3.8 cm diam stainless steel mesh cathode K, pass through the anode foil, and form a virtual cathode VC between A and G. Some of the electrons pass through VC to reach G and the rest reflex through A until they are absorbed in the anode or are lost to the walls of the anode stalk. Protons are extracted out of the plasma which is formed from the plastic anode. When the applied voltage is increasing or unchanging, protons directed toward VC are unable to reach G or reach G with zero velocity. Thus, these protons do not represent an energy drain on the system. However, most of the ions emitted toward K pass through the 75% transparent screen and enter the drift region.

Virtual cathode formation is an important process in this device and depends upon the uncompensated space charge distribution and the boundary conditions. The potential on axis $\phi(0,z)$ is plotted in Fig. 2a for a

radially uniform net charge density of radius r_b = 2.5 cm of the form $\rho(z) = \rho_1$ for $0 \leq z \leq d$ and $\rho(z) = \rho_2$ for $d < z \leq L$ with the boundary conditions $\phi(r,0) = \phi(r,L) = \phi(r_w,z) = V_o$ and $\phi(0,d) = 0$. For V_o = 500 kV, r_w = 5cm, L = 5 cm (solid line), $n_1 = \rho_1/e = 2 \times 10^{11} cm^{-3}$ and $n_2 = 1.28 \times 10^{11} cm^{-3}$, a virtual cathode is formed at $z \approx 2$ cm. However, when L is decreased to 2.5 cm and n_1 is unchanged (dashed line), no virtual cathode is formed. This behavior explains the experimental result (Fig. 2b) that proton production drops rapidly as A-G is decreased below $\sim$ 4 cm.

The number of protons N_p with E > 278 keV (as determined by nuclear activation of BN targets via $^{14}N(p,\gamma)^{15}O$ reactions) extracted from the IRT is found to be relatively insensitive to B_o for $B_o \lesssim 7$ kG (the highest field used), provided that an appropriate thickness anode foil is used. In Fig. 3, N_p vs. B_o is plotted for various foil thicknesses δ for both conical and cylindrical anode stalks. In both cases A-G $\approx$ 7.5 cm. The conical anode closely parallels the fringing external field and is found to generally provide higher N_p than the cylindrical anode. Also, too thin (12.5 μm) or too thick (250 μm) an anode foil clearly hinders proton production, especially at higher magnetic fields.

To understand this behavior, it is necessary to examine the voltage and current waveforms for the various cases. Typical waveforms obtained using the conical anode on the SOL generator are shown in Fig. 4. In general, the impedance of the IRT is higher and the current rise is slower at lower magnetic fields. Correspondingly, the voltage is relatively flat. As B_o is increased, the current rises more rapidly and a significant dip appears in the voltage trace. The current rise is also larger for δ between 25 and 100 μm. The depth and duration of the voltage dip increases with B_o up to a

point that depends on δ. For a particular B_o, the minimum value of the voltage in the dip V_{min} is higher for thicker anode foils. In fact, when the range of an electron of energy eV_{min} is reduced to approximately the foil thickness, no further decrease in V_{min} is observed as B_o is increased. When $B_o \gtrsim 7$ kG and $\delta = 250$ μm, the voltage dip disappears and the waveforms are similar to those in the 1-D simulation of Sternlieb et al.[13] Finally, it is found that with all other parameters fixed, the current rises more slowly and the voltage dip is less pronounced with the cylindrical than with the conical anode stalk.

The rapid initial current rise observed with the IRT is characteristic of reflexing electron devices.[7,8,11-13] The rise is due to a bootstrapping effect which occurs as the electrons reflex through the anode foil. The reflexing electrons form a negative charge cloud near the anode which draws ions from the anode plasma. The ions near the cathode further enhance electron emission, and the total current rises rapidly as the process continues. The reduction in the initial current rise with decreasing magnetic field is apparently due to a reduction of this bootstrapping effect. The self magnetic field B_{self} acts to inhibit the axial motion of the electrons when $B_o \ll B_{self}$. Also, when B_o is small, the limiting current in the A-G region increases[14] so that virtual cathode formation is more difficult and a higher electron current is lost to the end plate G or the walls of the anode stalk. These electron losses reduce the bootstrapping effect.

The slower current rise when $\delta \gtrsim 125$ μm is easily explained by the reduction in the number of electron transits N with increasing δ. If the foil is too thin, anode plasma production may be slowed because of the slower deposition of electrons in the anode foil. However, once a

sufficiently dense plasma is produced, the current rises very rapidly to a large value because N is quite large and bootstrapping is enhanced.

To explain the voltage dip, which has also been observed in a reflex triode experiment,[7] we must consider the external circuit to which the IRT is coupled.[8,13] The circuit equation is (see Fig. 1)

$$V_g = V_d + R_g I + L_g dI/dt \qquad (1)$$

where R_g and L_g are the resistance and inductance of the generator, V_d and I are the diode voltage and total current, and V_g is the open circuit generator voltage which is approxiamtely constant after an initial rise. Before anode plasma formation, the diode impedance is large and V_d rises quickly to a large value ($\sim$ 400 kV). If δ and B_o are such that the current rise is very rapid, the resistive and inductive terms in Eq. (1) become so large that V_d must decrease since V_g is constant ($\sim$ 600 kV). As V_d drops, N decreases and the bootstrapping effect is halted. For the lower magnetic fields, the current rise is slow enough so that V_d can remain approximately constant.

For large B_o, the diode voltage continues to drop until the electrons emitted from the cathode can penetrate the anode foil only once. As the electrons already in the device are absorbed by the anode foil, the negative charge cloud near the anode is rapidly reduced and the total current drops. The current drop is more rapid with thicker foils, because the electron absorption by the foil is faster. As dI/dt becomes negative, V_d must increase to satisfy Eq. (1). Then N becomes larger and I levels off. The diode voltage rise is then halted and there is a period of $\sim$ 15-20 ns during which $V_d \gtrsim 278$ kV. The magnitude of this second V_d peak is not a strong function of foil thickness. For example, at $B_o \gtrsim 7$ kG, $V_d \gtrsim 400$ kV

for foil thicknesses ranging from 50 μm to 125 μm. When both elastic and inelastic scattering are accounted for, the number of electron transits for such thickness foils is $N \approx 13\text{-}6$.

The better performance of the IRT with the conical than with the cylindrical anode stalk could be due to a lower electron loss to the walls of the conical stalk or to G. The B_o field lines intersect the walls of the cylindrical stalk so electrons can stream to the walls near the anode. Also, virtual cathode formation and the current I_t transmitted to G are affected by the wall shape. The cylindrical walls are closer to the beam radius, so the limiting current (and hence I_t) is larger.

Although $\sim$ 25% of the protons are stopped by the K screen, the efficiency ε of the IRT in its optimum operating regime is slightly larger than the theoretical value for reflex triodes:[12]

$$\varepsilon \equiv I_p/I = 0.5\ [1 + (2N + 1)^{-1}(m_i/m_e)^{\frac{1}{2}}]^{-1}\ , \qquad (2)$$

where I_p is the extracted proton current and $m_i(m_e)$ is the ion (electron) mass. Typical efficiencies obtained with δ = 50-100 μm and B_o = 2-7 kG are in the range 20-25%, while the theoretical values of ε vary from 15-20%. The efficiencies obtained here are a factor of two smaller than previous results with a reflex tetrode.[9] However, both N_p and $\langle I_p \rangle$ are about 1.5 times larger with the IRT than with the tetrode. This is because the IRT performs well at a much lower impedance (and hence higher current level) and is better matched to the generator than the reflex tetrode.

The authors appreciate the technical assistance of R. Covington, R. Welsh, and B. Hunicutt. This work was supported by ONR and DOE.

References

a) Sachs/Freeman Associates, Inc., Bladensburg, MD.

1. C.A. Kapetanakos, J. Golden, and F.C. Young, Nucl. Fusion 16, 161 (1976); C.A. Kapetanakos et al, Proc. of 2nd Int'l. Top. Conf. on High Power Electron and Ion Beam Res. & Tech., Cornell University, p. 435 (1977); H.H. Fleischmann, Proc. of Int'l. Top. Conf. on Electron Beam Res. & Tech., Sandia Laboratories, 2, 129 (1975); S. Humphries, Plasma Physics 17, 973 (1975), for example.
2. M.J. Clauser, Phys. Rev. Lett. 35, 848 (1975); F. Winterberg, Nature 251, 44 (1974); J. Shearer, Nucl. Fusion 15, 952 (1975) for example.
3. J. Golden, J.G. Eden, R.A. Mahaffey, J.A. Pasour, A.W. Ali, and C.A. Kapetanakos, Appl. Phys. Lett. 33, 143 (1978); J.G. Eden, J. Golden, R.A. Mahaffey, J.A. Pasour, and R.W. Waynant, Appl. Phys. Lett. 35, 133 (1979).
4. E. Ott and W.M. Manheimer, Nucl. Fusion 17, 1057 (1977).
5. S. Humphries, T.J. Lee, and R.N. Sudan, Appl. Phys. Lett. 25, 20 (1974).
6. C.A. Kapetanakos, J. Golden, and W.M. Black, Phys. Rev. Lett. 37, 1236 (1976); J. Golden, S.J. Marsh, C.A. Kapetanakos, and S. Stephanakis, Phys. Rev. Lett. 38, 130 (1977).
7. D.S. Prono, J.M. Creedon, I. Smith, and N. Bergstrom, J. Appl. Phys. 46, 3310 (1975); D.S. Prono, J.W. Shearer, and R.J. Briggs, Phys. Rev. Lett. 37, 21 (1976).
8. G. Cooperstein, S.A. Goldstein, J.J. Condon, D.D. Hinshelwood, D. Mosher, and S.J. Stephanakis, Bull. Am. Phys. Soc. 23, 800 (1978).
9. J.A. Pasour, R.A. Mahaffey, J. Golden, and C.A. Kapetanakos, Phys. Rev. Lett. 40, 448 (1978); R.A. Mahaffey, J.A. Pasour, J. Golden, and C.A.

Kapetanakos, Appl. Phys. Lett. 32, 522 (1978).

10. F. Wessel and S. Robertson, Appl. Phys. Lett. 34, 7 (1979).

11. T.M. Antonsen, Jr. and E. Ott, Phys. Fluids 19, 52 (1976) and T.M. Antonsen, Jr. and E. Ott, Appl. Phys. Lett. 28, 424 (1976).

12. J. Golden, C.A. Kapetanakos, R. Lee, and S.A. Goldstein, Proc. of Int'l. Top. Conf. on Electron Beam Res. & Tech., Sandia Laboratories, 1, 635 (1975).

13. A. Sternlieb, Shyke A. Goldstein, and Roswell Lee, University of Maryland Technical Report No. 79-059, Dec. 1978.

14. L.E. Thode, B.B. Godfrey, and W.R. Shanahan, Phys. Fluids 22, 747 (1979).

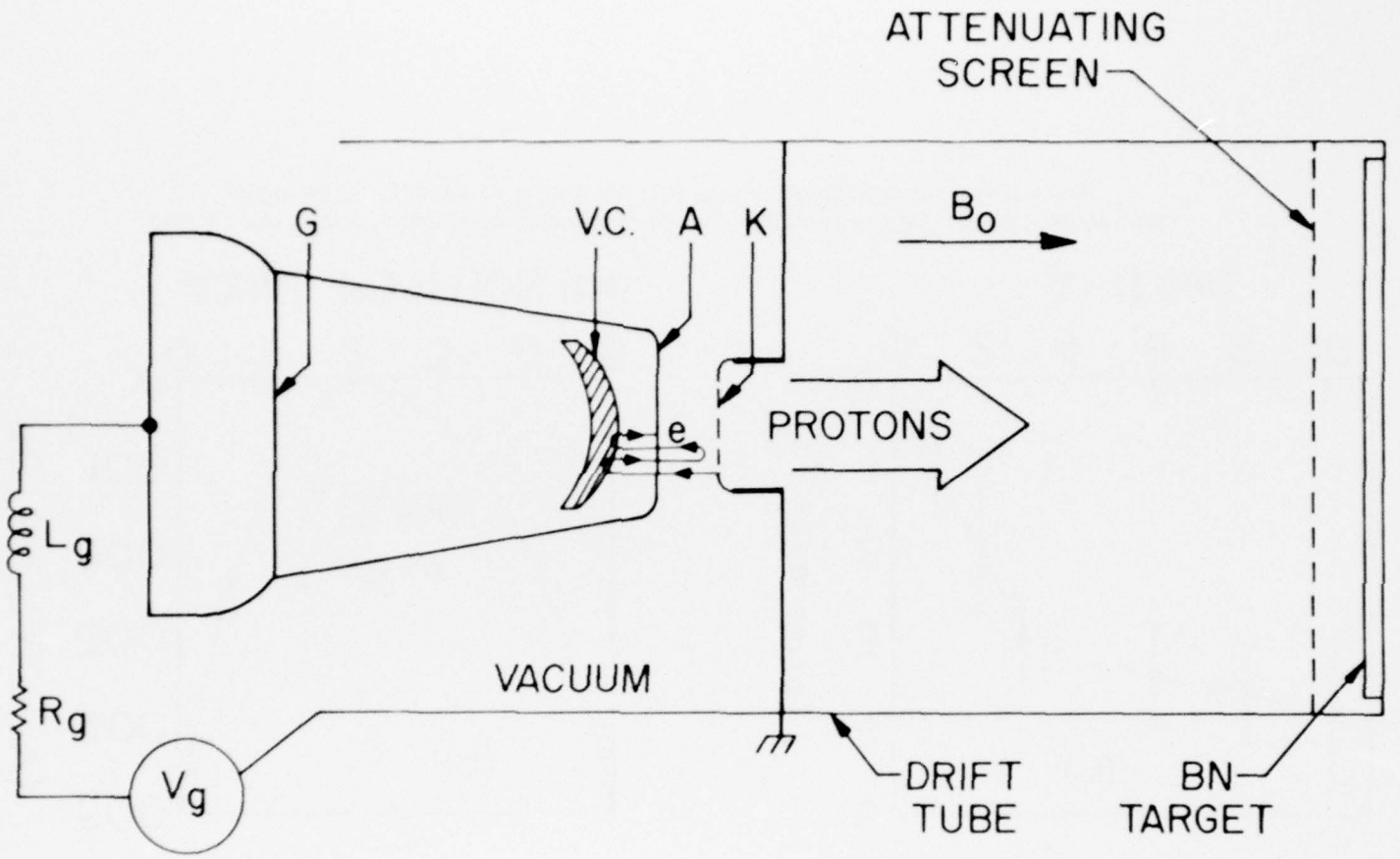

Fig. 1 — Schematic of IRT coupled to external generator

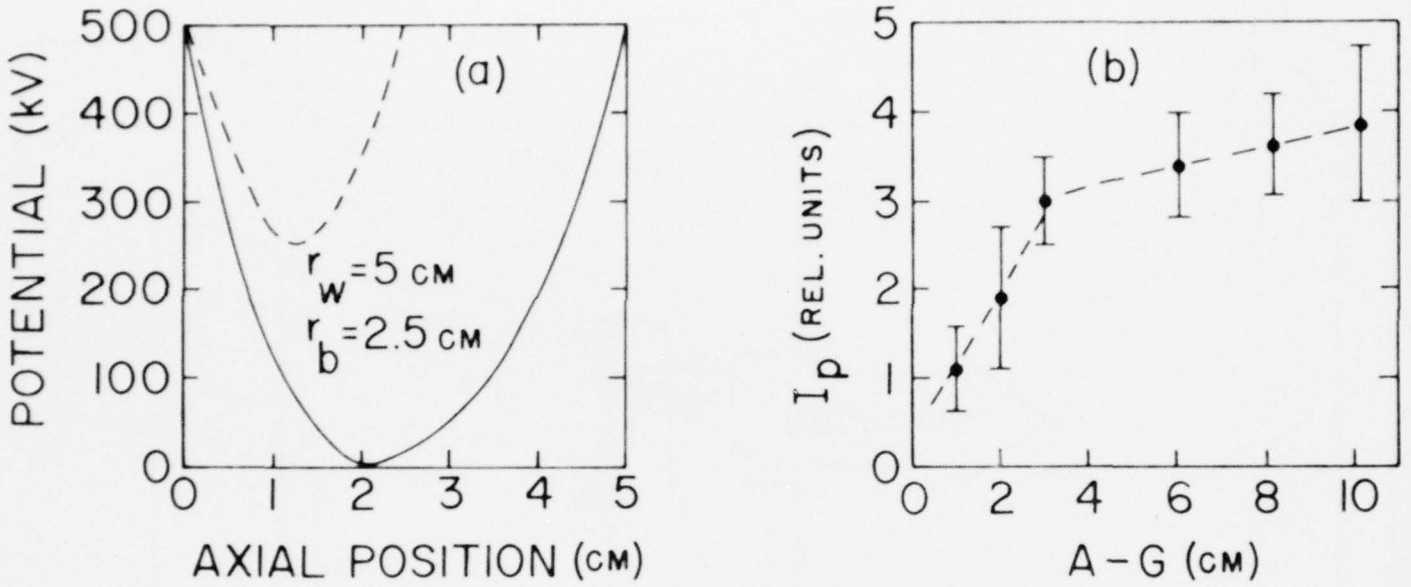

Fig. 2 — (a) Potential distribution on axis in the A-G region of an IRT. Solid (dashed) line is for an A-G spacing of 5(2.5) cm. (b) Proton production vs. A-G spacing.

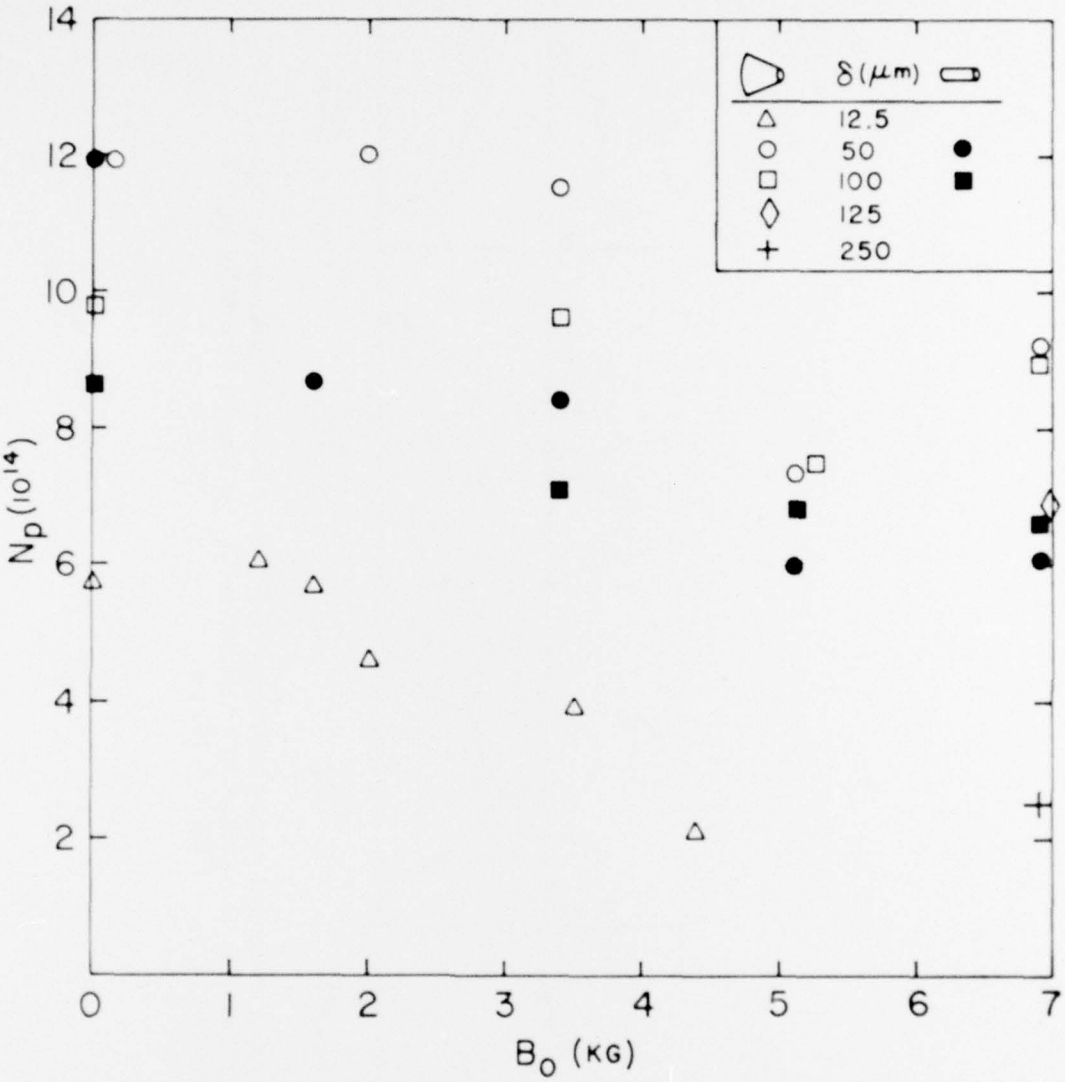

Fig. 3 — Proton production vs. B_0 for several anode foil thicknesses and for both conical and cylindrical anode stalks. Data points are subject to a statistical error of ~ 10-20%.

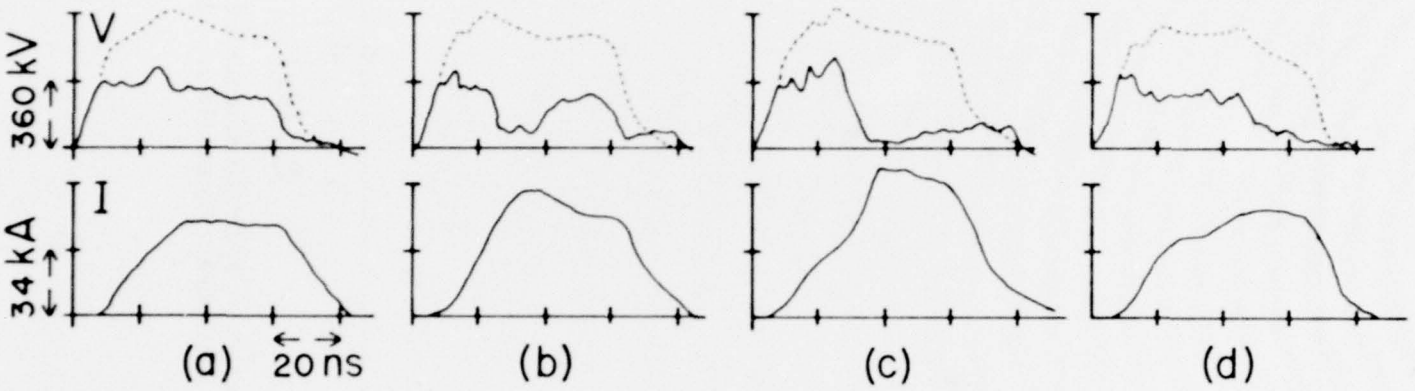

Fig. 4 — Typical voltage and current waveforms. Solid (dashed) voltage traces are V_d (V_g, as computed from Eq. 1). (a) $B_o = 0$, $\delta = 50\ \mu m$; (b) $B_o = 2$ kG, $\delta = 50\ \mu m$; (c) $B_o = 2$ kG, $\delta = 12.5\ \mu m$; (d) $B_o = 7$ kG, $\delta = 250\ \mu m$.